Near-field optical observations of surface plasmon wave interference at subwavelength hole arrays perforated in Au film*

Li Jiang-Yan(李江艳)[a)†], Gan Lin(甘 霖)[b)], and Li Zhi-Yuan(李志远)[b)‡]

[a)] *International Center for Quantum Materials, Peking University, Beijing* 100871, *China*
[b)] *Laboratory of Optical Physics, Institute of Physics, Chinese Academy of Sciences, Beijing* 100190, *China*

(Received 14 May 2013; revised manuscript received 10 August 2013)

We image optical near-field patterns at subwavelength circular hole arrays in Au film by using scanning near-field optical microscopy in near-infrared wavelengths. Periodical oscillation features are found in the near-field images at the air/Au interface and exhibit two typical kinds of standing wave oscillation forms at the wavelengths corresponding to the transmission minimum and maximum in the transmission spectrum, and the latter one originates from the excitation and interference of a surface plasmon wave at the metallic hole arrays. Our work indicates that monitoring optical near-field patterns can help to reveal many interesting properties of surface plasmon waves at metallic nanostructures and understand their underlying physical mechanisms.

Keywords: surface plasmon waves, near-field pattern, oscillation

PACS: 73.20.Mf, 07.79.Fc, 52.35.Fp **DOI:** 10.1088/1674-1056/22/11/117302

1. Introduction

In recent years, interaction between light and subwavelength metallic nanostructures has aroused great interest and a lot of surprising phenomena have been found. Extraordinary light transmission through subwavelength hole arrays was first found by Ebbesen and coworkers in 1998,[1] and directional beam collimation of light by apertures dressed with subwavelength grooves was first reported by Lezec and coworkers in 2002.[2] From then on, many experimental and theoretical studies[3–16] have been made to understand these phenomena and surface plasmon polaritons (SPPs) have been found to be an important contributing factor. A surface plasmon wave, created by an individual metallic nanostructure, will interact with other nanostructures to build up observed SPP phenomena.[17] Far-field imaging of surface plasmon waves scattered by metal nanostructures has been carried out extensively,[18,19] which can help to reveal wave propagation direction and oscillation period. However, near-field observations will be more helpful because surface plasmon waves are bound at the metal–dielectric interface and far-field imaging only shows the scattering situation of interaction.

A scanning near-field optical microscope (SNOM) can break the diffraction limit of the resolution of light to recover evanescent wave information[20,21] and many near-field experiments on metal nanostructures have been done.[22–25] Near-field images on a single metal nanoaperture,[26] metal double slits,[27] and metal apertures dressed with subwavelength grooves[27] all show interference patterns, which result from the interaction of surface plasmon waves. Two-dimensional (2D) subwavelength hole arrays perforated in metal films have complicated geometric structures and can sustain different surface plasmon modes. It will be useful to image near-field patterns at 2D metal subwavelength hole arrays in order to understand the physics of SPP.

In this work, we report our measurement of near-field patterns at the air/Au interface at periodic subwavelength hole arrays by using an SNOM, where the data are obtained every several nanometers in the range of 1500–1640 nm. The periodicity of the near-field patterns is fairly good and oscillation structures are found to exist in the near-field images. Analysis of the measured near-field patterns shows the existence of two kinds of oscillation forms, which can transform from one form to the other when the wavelength changes. The transmission spectrum and the near-field patterns are also simulated by using the plane-wave transfer-matrix method (PWTMM)[28,29] for better understanding the experimental observations. It was found that the two kinds of oscillation forms correspond to the situations where the transmission minimum and maximum of light through the nanostructured gold thin film take place. The experimental results also show that change of lattice constant of the hole array has some effects on the wavelength where the two kinds of oscillation forms take place.

2. Sample preparation and experimental setup

The subwavelength hole arrays were fabricated by Raith 150 electron-beam lithography (EBL) and then by

*Project supported by the National Basic Research Program of China (Grant Nos. 2011CB922002 and 2013CB632704) and the Knowledge Innovation Program of the Chinese Academy of Sciences.

†Corresponding author. E-mail: yanr163@163.com
‡Corresponding author. E-mail: lizy@aphy.iphy.ac.cn

© 2013 Chinese Physical Society and IOP Publishing Ltd

reactive-ion-beam etching (RIE) technology in a 100-nm-thick (optically-thick) Au film deposited on quartz substrate. Circular hole arrays arranged in a square lattice are considered and the hole radius is 0.5 μm, while the lattice constant is 3.05 μm, 3.08 μm, and 3.1 μm, respectively. A typical scanning electron microscope (SEM) image of the fabricated samples is shown in Fig. 1(a). The overall size of each array is about 100 μm × 100 μm.

In the near-field measurement system, an SNOM (NSOM-100 Nanonics, Israel) operating in collection mode is used. The light source is a continuous semiconductor laser which is tunable from 1500 nm to 1640 nm with the maximum output power of about 10 mW. The light intensity at each scanning observation point is measured using an Au-coated fiber probe with 150-nm apertures operating at 10 nm above the metal film. In the usual collection mode, the sample is illuminated by the microscope objective of the SNOM. As a result, the incident light is a focused light beam with a certain collection angle determined by the numerical aperture of the objective. As we are interested in the problem of a normal incidence of plane-wave light, we implement a slight modification to the apparatus. The light from the semiconductor laser is launched into an ordinary single-mode fiber and illuminates the sample on the substrate side from the other end of the fiber that is placed perpendicularly to the sample. As the fiber end is placed in close proximity to the substrate surface, the approximation of the condition of plane-wave illumination can be satisfied to a good degree. The experimental local setup of SNOM is schematically shown in Fig. 1(b). The incident plane-wave light illuminates the sample perpendicularly and the aperture probe coated with metal film collects the near-field signal of light above the metal film. Meanwhile, linearly polarized light is used by the optical fiber polarizer. In the simulation, we use the same plane-wave illumination and sample structure as in the experimental setup. In addition, the experimentally measured dispersion data (including the real and imaginary parts of permittivity) of gold[30] have been used in the PWTMM simulation. The transmission spectrum and near-field patterns of the circular hole array at the air/Au interface are simulated by PWTMM. The interaction and perturbation between the SNOM tip and the surface of the plasmonic structure are not considered in the simulation, where the metallic tip collects information about the electric field intensity at 10 nm above the metallic surface in the measurement. This problem has been studied in Ref. [31] experimentally and numerically, which has compared the electric field intensity distribution at the metallic surface with and without tip. The results show that the tip will influence the near-field intensity, but has no influence on the near-field phase. However, this influence should depend on the geometric details of the SNOM tip, which is not available in our SNOM system. Therefore, in the current work we only compare the profile of the electric field intensity distribution between the measured results and the simulated results without tip, and make an approximate assumption that the SNOM tip can reflect the near-field pattern in the SPP phase without or with less perturbation from the tip.

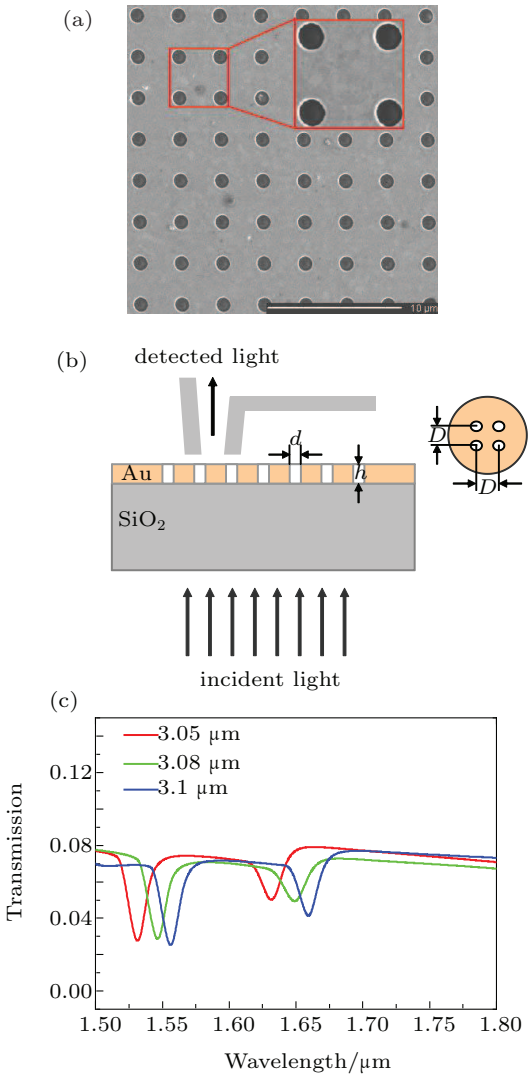


Fig. 1. (color online) (a) A typical scanning electron microscope image of the circular hole array samples. The lattice constant of the circular hole array is 3.1 μm and the hole radius is 0.5 μm. (b) Schematic of the experimental local setup image of the SNOM. (c) Simulated transmission spectrum of the samples at wavelengths ranging from 1.5 μm to 1.8 μm using the plane-wave transfer matrix method (PWTMM). The hole radius of the circular hole arrays is 0.5 μm, while the lattice constant is 3.05 μm, 3.08 μm, and 3.1 μm, respectively.

3. Results and discussion

The transmission spectra at the subwavelength circular hole arrays of different lattice constants are simulated by the PWTMM and shown in Fig. 1(c). Higher order transmission minimums and maximums are found in the spectra, which are located at 1530 nm and 1565 nm, 1545 nm and 1585 nm, 1555 nm and 1595 nm in the wavelength range of 1500–1640 nm for the samples with lattice constants of 3.05 μm,

3.08 μm, and 3.1 μm, respectively. These higher-order minimum and maximum transmissions existing in the calculated transmission spectrum are not measured experimentally because of the very weak transmission intensity of these transmission abnormalities and the presence of noise in the measurement setup.

The measured near-field patterns of the circular hole array sample at different wavelengths are shown in Fig. 2. The lattice constant of the array is 3.05 μm and the hole radius is 0.5 μm. The periodicity of the near-field distribution is fairly good, which suggests that this metallic sample is satisfactorily uniform in the whole scanning area and that the incident light is a plane wave that excites the whole metallic structure uniformly. Apparent oscillation structures exist in all the near-field images and four stripes are found along the x axis within one unit cell. Obviously, there are two kinds of oscillation forms at wavelengths of 1538 nm and 1560 nm, respectively. Three stripes extend all over one unit cell in the y axis in the near-field image at wavelength of 1538 nm, while at wavelength of 1560 nm three stripes also exist but are more localized around the holes in the near-field image. The near-field patterns at wavelengths of 1540 nm, 1545 nm, and 1550 nm show a departure from that at a wavelength of 1538 nm and a gradual transformation to that at wavelength of 1560 nm. The near-field patterns at wavelengths of 1570 nm and 1575 nm show a departure from that at a wavelength of 1560 nm.

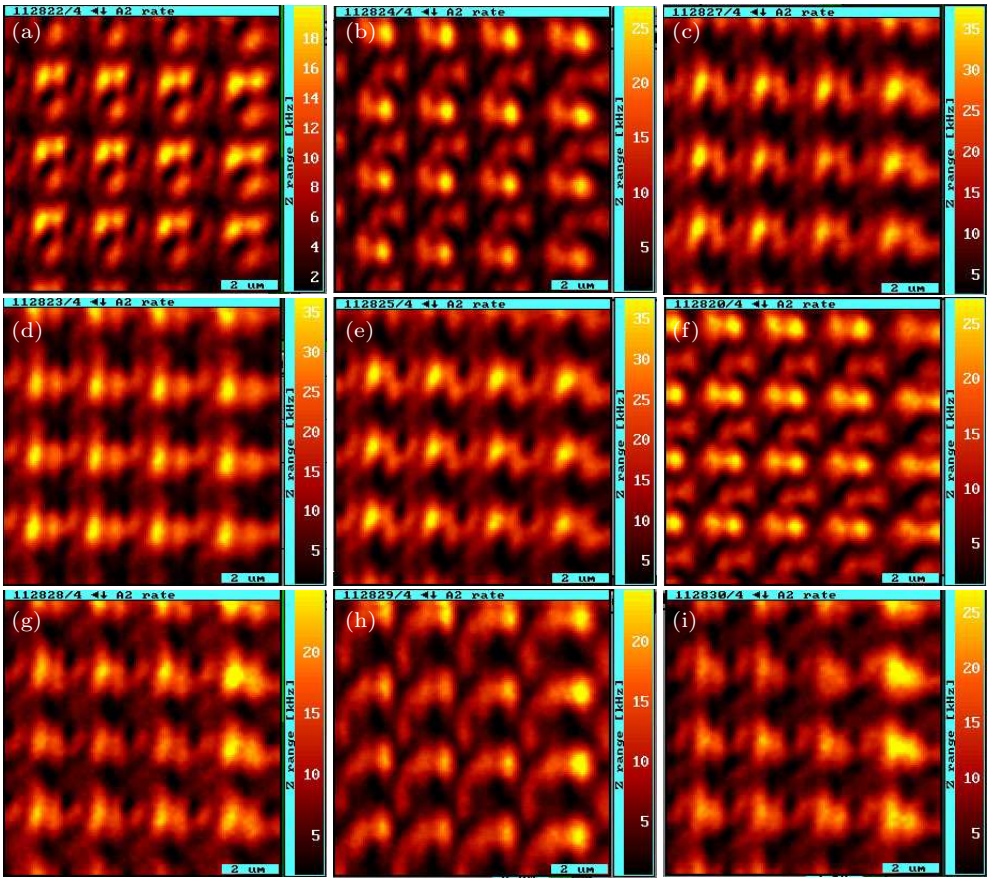


Fig. 2. (color online) Measured near-field patterns of the circular hole array sample at different wavelengths of (a) 1530 nm, (b) 1535 nm, (c) 1538 nm, (d) 1540 nm, (e) 1545 nm, (f) 1550 nm, (g) 1560 nm, (h) 1570 nm, and (i) 1575 nm by the SNOM. The lattice constant is 3.05 μm and the hole radius is 0.5 μm. The polarization of the incident light is in the x axis and the scalar bar (2 μm) is marked in the near-field images. Note that this scale bar is unrevised because the size inaccuracy due to the positioning nonlinearity of our SNOM is not corrected, and the scanning range is different from the value measured by the SEM. To get the correct scale bar of the SNOM optical image, we need to refer to the SEM image of the same sample. Two kinds of oscillation forms take place at wavelengths of 1538 nm and 1560 nm, respectively.

The simulated transmission minimum and maximum of the array sample are located at wavelengths of 1530 nm and 1565 nm, respectively, which is close to 1538 nm and 1560 nm as deduced from the measured near-field patterns in the accepted range of deviation between experimental results and theoretical results. The simulated near-field patterns at wavelengths of 1530 nm and 1565 nm attached with measured near-field patterns at wavelengths 1538 nm and 1560 nm are shown in Fig. 3. About 4×4 periods exist in Figs. 3(a) and 3(b) and 2×2 periods are present in Figs. 3(c) and 3(d). General agreement between the measured and simulated results has been achieved. First, there are bright spots around the hole in the measured near-field images, which are also seen in the simulated pictures. Second, there are interference-like stripe

structures in both the measured and simulated images. Third, both the measured and the simulated results show better field localization in the patterns in Figs. 3(a) and 3(c) compared with those in Figs. 3(b) and 3(d). Fourth, the stripes extend into an adjacent period along the y axis in the theoretical results in Fig. 3(d), the same as that in the measured results in Fig. 3(b). However, some differences also appear between the experiment and the theory, one of which is the interference period number. Four stripes and four oscillation periods exist in the simulated results, but three stripes and three oscillation periods exist in the measured results for both wavelengths. In view of the stretching effect of the 150-nm aperture probe, and especially of the interaction and perturbation of metallic filming tip-sample distance at 10 nm, we believe that the two adjacent darker stripes that correspond to weaker field intensity at the borderline of one periodical cell in the theoretical result assemble together into one single stripe with a larger width in the measured result. This stripe extends into adjacent unit cells at a wavelength of 1538 nm, while remains well localized within one unit cell at 1560 nm. Such measured near-field features agree well with the simulated results.

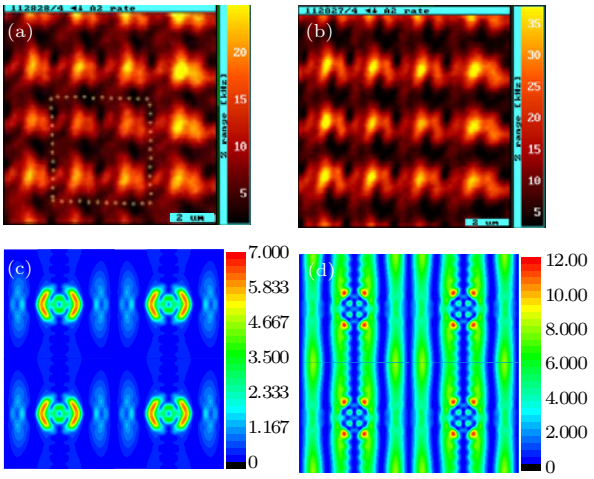


Fig. 3. (color online) Measured and simulated near-field patterns of the circular hole array sample with a lattice constant of 3.05 μm and a hole radius of 0.5 μm. (a) Measured near-field patterns at a wavelength of 1560 nm. (b) Measured near-field patterns at a wavelength of 1538 nm. (c) Simulated near-field patterns at a wavelength of 1565 nm, which corresponds to the transmission maximum in the simulated transmission spectrum. (d) Simulated near-field pattern at a wavelength of 1530 nm, which corresponds to the transmission minimum in the simulated transmission spectrum. One period is marked by a yellow square and the standing wave period is about $\lambda_{sw} \sim 0.763$ μm, as can be extracted from panel (a). The incident light polarization is along the x axis and the scalar bar marked in (a) and (b) is also unrevised.

In view of previous studies,[3–14] we believe that the oscillation structure in the measured near-field image at 1560 nm wavelength originates from the interference of surface plasmon waves propagating in opposite directions and scattered by the periodic array of air holes, which leads to a maximum in the transmission spectrum. In comparison, the oscillation structure in the measured near-field image at 1538 nm wavelength corresponding to the minimum in the transmission spectrum may be induced by the interference of diffraction surface waves associated with Wood's anomaly. We can deduce from a more detailed one-dimensional profile of the measured near-field pattern in Fig. 3(a) that the standing wave period is $\lambda_{sw} \approx 0.763$ μm. The standing wave results from interference of surface plasmon waves scattered by adjacent holes, which is depicted as $E_{spw} \sim A \exp(-|x|/2\sigma) \exp(\mathrm{i}k_{spp}x)$ and $k_{spp} = 2\pi/\lambda_{spp}$. Interference of two surface plasmon waves with k_{spp} and $-k_{spp}$ yields $\lambda_{sw} = \lambda_{spp}/2$, so $\lambda_{spp} \sim 1.526$ μm. In view of the SPP dispersion relation $k_{spp} = (2\pi/\lambda_0)[\epsilon_m \epsilon_d/(\epsilon_m + \epsilon_d)]^{1/2}$, where ϵ_m and ϵ_d are the dielectric constant of air and gold at this specific wavelength, the surface plasmon wavelength is about 1.55 μm at the illumination wavelength of 1560 nm. This value is close to 1.526 μm as deduced from the measured near-field pattern at wavelength 1560 nm. Therefore, the measured near-field pattern at wavelength of 1560 nm should correspond to the excitation of the surface plasmon wave $(2,0)$ mode and $(-2,0)$ mode, according to the momentum conservation relation at the metal subwavelength hole array, i.e., $\boldsymbol{k}_{spp} = \boldsymbol{k}_{0//} + m\boldsymbol{G}_x + n\boldsymbol{G}_y$.

The near-field patterns of the circular hole array sample of lattice constant 3.08 μm are also measured using the SNOM and we pick out two kinds of interference forms at wavelengths of 1530 nm and 1590 nm, respectively. The wavelengths of the transmission minimum and maximum in the simulated transmission spectrum in Fig. 1(b) are 1545 nm and 1585 nm, which are close to the wavelengths in the measured results. The simulated near-field patterns at wavelengths of 1545 nm and 1585 nm, attached with the measured near-field patterns at wavelengths of 1530 nm and 1590 nm are shown in Fig. 4. Almost 4×4 periods exist in Figs. 4(a) and 4(b) and 2×2 periods are present in Figs. 4(c) and 4(d). General agreement between the measured and simulated results has been achieved. The field patterns are similar to those displayed in Fig. 3. Better localization of field around the holes is also achieved in Figs. 4(a) and 4(c) compared with Figs. 4(b) and 4(d). There are three stripes in the measured pattern in Figs. 4(a) and 4(b) as opposed to four stripes in the theoretical pattern in Figs. 4(c) and 4(d). The difference in the interference period number also results from the stretching effect of the aperture probe of the SNOM. The extension of the darker stripe along adjacent unit cells along the y axis is more apparent in Fig. 4(b) than in Fig. 3(b). The bright spots around the hole against the dark stripe at the borderline are very apparently resolved. The standing wave pattern at 1590 nm wavelength results from the interference of the surface plasmon wave scattered by adjacent holes. We can deduce $\lambda_{sw} \sim 0.77$ μm and $\lambda_{spp} \sim 1.54$ μm from the standing wave pattern at wavelength of 1590 nm. Meanwhile, the surface plasmon wavelength is about 1.58 μm, as deduced from

the dispersion relation of surface plasmon wave at the illumination wavelength of 1590 nm, which is close to 1.54 μm as deduced from the measured near-field patterns at wavelength of 1590 nm. The measured near-field pattern at wavelength of 1590 nm also corresponds to the excitation of the surface plasmon wave $(2,0)$ mode and $(-2,0)$ mode.

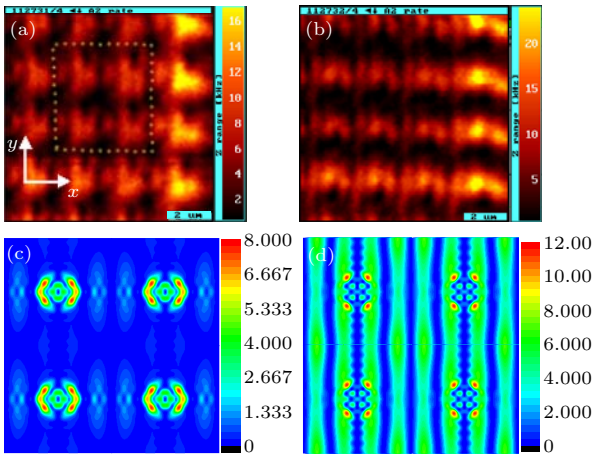


Fig. 4. (color online) Measured and simulated near-field patterns of the circular hole array sample with the lattice constant being 3.08 μm and the hole radius 0.5 μm. (a) Measured near-field patterns at wavelength of 1590 nm. (b) Measured near-field patterns at wavelength of 1530 nm. (c) Simulated near-field patterns at wavelength of 1585 nm, which corresponds to the transmission maximum in the simulated transmission spectrum. (d) Simulated near-field pattern at wavelength of 1545 nm, which corresponds to the transmission minimum in the simulated transmission spectrum. One period is marked by a yellow square and the standing wave period is about λ_{sw} ~0.77 μm, as is extracted from panel (a). The incident light polarization is along the x axis and the scalar bar marked in (a) and (b) is also unrevised.

The near-field patterns of the circular hole array sample with lattice constant 3.1 μm are also measured using the SNOM and we pick out two kinds of interference forms at wavelengths of 1540 nm and 1600 nm. The simulated transmission spectrum in Fig. 1(b) shows that the transmission minimum and maximum are located at wavelengths of 1555 nm and 1595 nm, respectively, which are close to the measured results. The simulated near-field patterns at wavelengths of 1555 nm and 1595 nm, attached with measured near-field patterns at wavelengths of 1540 nm and 1600 nm are shown in Fig. 5. General agreement between measured and simulated results has also been achieved. Better localization is also achieved in Figs. 5(a) and 5(c) compared with Figs. 5(b) and 5(d). The stretching effect of the SNOM aperture probe also takes place here, leading to the merger of the two weak stripes in Figs. 5(c) and 5(d) into one stripe in Figs. 5(a) and 5(b), which is now much clearer than Fig. 3(b). The two bright spots around the holes, which appear in the simulated results shown in Figs. 5(c) and 5(d), are now clearly recovered experimentally.

The standing wave pattern in the near-field pictures at wavelength 1600 nm also results from the interference of surface plasmon wave scattered by adjacent holes. Detailed analysis on the experimental and theoretical data indicates that $\lambda_{sw} \sim 0.775$ μm and $\lambda_{spp} \sim 1.55$ μm. The surface plasmon wavelength is about 1.59 μm as deduced from the dispersion relation of the surface plasmon wave at the illumination wavelength of 1600 nm, which agrees with the value as extracted from the measured near-field standing wave pattern. Furthermore, the measured near-field pattern at wavelength of 1600 nm also originates from the excitation of the surface plasmon wave $(2,0)$ mode and $(-2,0)$ mode.

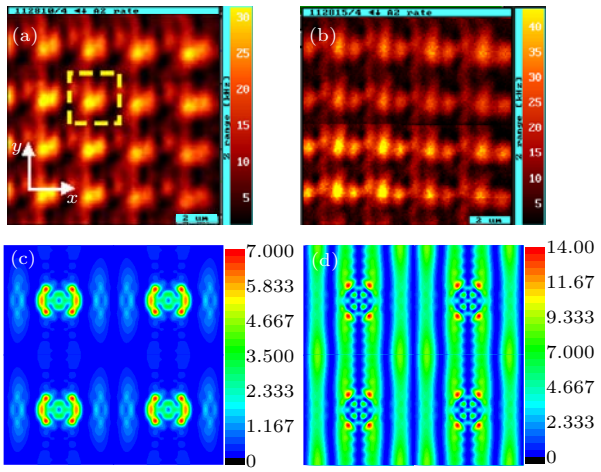


Fig. 5. (color online) Measured and simulated near-field patterns of the circular hole array sample with the lattice constant being 3.10 μm and the hole radius 0.5 μm. (a) Measured near-field patterns at wavelength of 1600 nm. (b) Measured near-field patterns at wavelength of 1540 nm. (c) Simulated near-field patterns at wavelength of 1595 nm, which corresponds to the transmission maximum in the simulated transmission spectrum. (d) Simulated near-field pattern at wavelength of 1555 nm, which corresponds to the transmission minimum in the simulated transmission spectrum. One period is marked by a yellow square and the standing wave period is about $\lambda_{sw} \sim 0.775$ μm, as is extracted from panel (a). The incident light polarization is along the x axis and the scalar bar marked in panels (a) and (b) is also unrevised.

The near-field studies on the circular hole arrays of lattice constant 3.05 μm, 3.08 μm, and 3.1 μm show the effect of the lattice constant on the wavelengths of two kinds of interference forms and also the wavelengths of the transmission minimum and maximum in the transmission spectrum. The period of the standing wave pattern are 763 nm, 770 nm, and 775 nm, corresponding to the lattice constant 3.05 μm, 3.08 μm, and 3.1 μm, respectively, which apparently grows when the lattice constant increases. The corresponding SPP wavelengths also increase when the lattice constant increases. This again verifies that the standing wave pattern originates from excitation and interference of SPP at the metallic nanostructure.

4. Conclusions

In conclusion, we have used an SNOM to study the near-field patterns at the surface of Au circular hole array samples of different lattice constants in the near-infrared light range.

The near-field images show a standing wave structure and interference stripes with different intensities. Two forms of interference exist in the measured near-field patterns and they transform from one form to the other when the incident light wavelength changes. The simulated transmission spectra of these arrays show that the wavelengths of the transmission minimum and maximum agree with those at which the two kinds of interference forms take place. Meanwhile, the surface plasmon wavelength can be deduced from the measured near-field patterns, which agrees with that deduced from the dispersion relation of surface plasmon wave. The measured near-field pattern is found to correspond to the excitation and interference of the surface plasmon wave $(2,0)$ mode and $(-2,0)$ mode. The high resolution near-field study by using an SNOM can help to extract detailed propagation pictures of an SPP at metallic nanostructures of subwavelength hole arrays, and it also helps to understand the physical mechanisms underlying these phenomena.

References

[1] Ebbesen T W, Lezec H J, Ghaemi H F, Thio T and Wolff P A 1998 *Nature* **391** 667

[2] Lezec H J, Degiron A, Devaux E, Linke R A, Martin-Moreno L, Garcia-Vidal F J and Ebbesen T W 2002 *Sciencee* **297** 820

[3] Salomon L, Grillot F, Zayats A V and de Fornel F 2001 *Phys. Rev. Lett.* **86** 1110

[4] Biswas R, Neginhal S, Ding C G, Puscasu I and Johnson E 2007 *J. Opt. Soc. Am. B* **24** 2589

[5] Liu H and Lalanne P 2008 *Nature* **452** 728

[6] Thio T, Ghaemi H F, Lezec H J, Wolff P A and Ebbesen T W 1999 *J. Opt. Soc. Am. B* **16** 1743

[7] Chang Y T, Yang C H, Tsai M W and Lee S C 2007 *Appl. Phys. Lett.* **90** 213101

[8] Kwak E S, Henzie J, Chang S H, Gray S K, Schatz G C and Odom T W 2005 *Nano. Lett.* **5** 1963

[9] Hecht B, Bielefeldt H, Novotny L, Inouye Y and Pohl D W 1996 *Phys. Rev. Lett.* **77** 1889

[10] Esteban R, Vogelgesang R, Dorfmuller J, Dmitriev A, Rockstuhl C, Etrich C and Kem K 2008 *Nano. Lett.* **8** 3155

[11] Chang S H, Gray S K and Schatz G C 2005 *Opt. Express* **13** 3150

[12] Bozhevolnyi S I and Coello V 1998 *Phys. Rev. B* **58** 10899

[13] Gay G, Alloschery O, de Lesegno B V, O'Dwyer C, Weiner J and Lezec H J 2006 *Nat. Phys.* **2** 262

[14] Lalanne P and Hugonin J P 2006 *Nat. Phys.* **2** 551556

[15] Mrejen M, Israel A, Taha H, Palchan M and Lewis A 2007 *Opt. Express* **15** 9129

[16] Sun M, Liu R J, Li Z Y, Feng S, Cheng B Y, Zhang D Z, Yang H F and Jin A Z 2006 *Phys. Rev. B* **74** 193404

[17] Aigouy L, Lalanne P, Hugonin J P, Julie G and Mathet V 2007 *Phys. Rev. Lett.* **98** 153902

[18] Tetz K A, Rokitski R, Nezhad M and Fainman Y 2005 *Appl. Phys. Lett.* **86** 111110

[19] Altewischer E, van Exter M P and Woerdman J P 2003 *J. Opt. Soc. Am. B* **20** 1927

[20] Tao H H, Liu R J, Li Z Y, Feng S, Liu Y Z, Ren C, Cheng B Y, Zhang D Z, Ma H Q, Wu L A and Zhang Z B 2006 *Phys. Rev. B* **74** 205111

[21] Li J Y, Li Z Y, Yang H F and Jin A Z 2008 *J. Appl. Phys.* **104** 114303

[22] Guestin L, Adam A J L, Knab J R, Nagel M and Planken P C M 2009 *Opt. Express* **17** 17412

[23] Liu C, Chen N and Sheppard C 2007 *Appl. Phys. Lett.* **90** 011501

[24] Wellems L D, Huang D, Leskova T A and Maradudin A A 2009 *J. Appl. Phys.* **106** 053705

[25] Krenn J R, Dereux A, Weeber J C, Bourillot E, Lacroute Y, Goudonnet J P, Schider G, Gotschy W, Leitner A, Aussenegg F R and Girard C 1999 *Phys. Rev. Lett.* **82** 2590

[26] Yin L, Vlasko-Vlasov V K, Rydh A, Pearson J, Welp U, Chang S H, Gray S K, Schatz G C, Brown D B and Kimball C W 2004 *Appl. Phys. Lett.* **85** 467

[27] Verhagen E, Dionne J A, Kuipers L, Atwater H A and Polman A 2008 *Nano Lett.* **8** 2925

[28] Li Z Y and Lin L L 2003 *Phys. Rev. E* **67** 046607

[29] Li Z Y and Ho K M 2003 *Phys. Rev. B* **68** 245117

[30] Palik E D 1985 *Handbook of Optical Constant of Solids* (Orlando: Academic Press)

[31] Wang J, Fu Y Q, Xu Z W and Fang F Z 2013 *Quantum Matter* **2** 289